



Assessment of adsorption performance of chitosan/ZrO₂ biosorbent composite towards Cs (I) and Co (II) metal ions from aqueous solution

G. A. Dakroury¹ · S. M. Ali¹ · H. S. Hassan²

Received: 5 July 2021 / Accepted: 12 September 2021 / Published online: 18 September 2021
© The Polymer Society, Taipei 2021

Abstract

Three different Chitosan/ZrO₂ (CTS-ZrO₂) composites are prepared by sol–gel then, used as bio-sorbent for Cs (I) and Co (II) metal ions from aqueous solution in this study. Characterization of (CTS-ZrO₂) composites is done through different analytical techniques. Optimizations of the adsorption affecting factors are explored via batch mode. The adsorption equilibrium attained after 60 min for initial metal ion concentration is 100 mgL⁻¹ and at optimum pH 9 and 6 for Cs (I) and Co (II), respectively. Kinetic modelling is applied and the adsorption reaction followed pseudo 2nd order. The adsorption capacity for Cs (I) at pH 9 and 25°C is 124.6 mgg⁻¹ and for Co (II) at pH 6 and 25°C is 111.1 mgg⁻¹. The thermodynamic parameters showed the adsorption reaction is spontaneous and endothermic.

Keywords Cs (I) · Co (II) · Adsorption · Chitosan · ZrO₂ · Biosorbent

Introduction

The rapid development in the use of nuclear power is inextricably linked to the generation and accumulation of liquid radioactive waste (LRW). Owing to the long $t^{1/2}$, high toxicity and carcinogenicity of these waste, a new effective technologies and materials for their safe management developed. Cs (I), Sr (II) and Co (II) ions are the basic fission products and present in almost all the contaminated radioactive wastewater [1].

These ions may have many benefits to human life. Early research suggests that Cs (I) joined with other vitamins, minerals, chelating agents and salts of selenium, potassium and magnesium. In addition, a special diet might reduce the death rate in some patients with various types of cancer [2]. However, high doses of Cs (I) might be unsafe. There are reports of severe life-threatening low blood pressure and irregular heartbeat in some people who took high doses of cesium for several weeks. Cs (I) deposited in the soft tissues

throughout the body and induce thyroid cancer. ¹³⁷Cs is a very dangerous isotope as it is a γ and β radiation source and its $t^{1/2}$ is relatively long about 30 years [3, 4].

Co (II) used as an alloy component in Electroplating [5]. High-energy γ rays emitted during the radioactive decay of ⁶⁰Co, used in treatment of various types of cancer. Adverse health effects, such as cardiomyopathy and vision or hearing impairment, reported at peak blood Co concentrations. Therefore, Cs (I), Sr (II) and Co (II) eliminated from contaminated liquid waste are in urgent need. Many approaches such as precipitation and coagulation methods [6, 7], Ion exchange [8, 9], Ultra filtration [10], reverse osmosis [11] and adsorption [12] are used for waste treatment. The latter method is the superior applied method due to its simplicity, economically, and feasibility. Inorganic, organic, and biological adsorbents could be used in adsorption techniques. The choice of adsorbents depends on the cost, efficiency and the environmental eco-friendly.

Chitosan (CTS) is a natural polymer emerging in the adsorption process [13–15]. In addition to its biocompatibility, it has many advantages as good adsorption capacity, biodegradability [16–19], environmentally safe and cheap compared to other adsorbents.

Metal ions introduction to CTS has recently been practiced for waste treatment in order to improve the mechanical properties and thermal stability properties of CTS [15]. e.g.,

✉ G. A. Dakroury
dr_gdakroury2010@yahoo.com

¹ Nuclear Chemistry Department, Hot Laboratories Centre, Egyptian Atomic Energy Authority, P.O. 13759, Cairo, Egypt

² Waste Management Department, Hot Laboratories Centre, Egyptian Atomic Energy Authority, P.O. 13759, Cairo, Egypt

zinc (II) [20] and copper (II) [21], are capable of forming complexes with the functional groups on the CTS chain.

Zirconium oxide (ZrO_2) is an inert inorganic metal oxide has chemical resistivity toward acids, bases, oxidants and reductants [22, 23]. It is envisaged that ZrO_2 enhances the properties of chitosan in chitosan / ZrO_2 composite [24] (CTS- ZrO_2).

However, to date, there is a limited study on CTS- ZrO_2 composites as adsorptive media for the removal of Cs (I) and Co (II).

This work aims to prepare Chitosan/ ZrO_2 composites (CTS/ ZrO_2). Characterization of CTS/ ZrO_2 composites is carried out by FTIR, SEM, XRD, Particle size analyzer, and TGA/DTA. Adsorption processes of Cs (I) and Co (II) ions on (CTS/ ZrO_2) composites are explained. Adsorption parameters effect such as; pH, temperature, contact time and initial metal concentration on metal ions are examined. The kinetics and isothermal models fitting are carried out and the thermodynamic nature of the adsorption reaction is studied.

Experimental

Reagents

Most of the chemicals were of analytical grade and used without further purification. Zirconium n-propoxide, $Zr(OC_3H_7)_4$, purity 70% obtained from Merck. Magnesium nitrate, $Mg(NO_3)_3 \cdot 6H_2O$, as a precursor for MgO supplied from Alfa Aesar and used as stabilizer for ZrO_2 . Chitosan with low molecular weight and deacetylation degree of 75–85% purchased from Sigma-Aldrich (USA). Acetic acid, (CH_3COOH), supplied from ADWIC (Egypt). Isopropyl alcohol, ($C_3H_8OH \geq 99.7\%$), obtained from Prolabo, England. Ammonium hydroxide, (NH_4OH), 33% from Edwic El-Nasr, Egypt. Hydrochloric acid, (HCl), and sodium hydroxide, (NaOH), obtained from El-Nasr Co. (ADWIC), Egypt, used to adjust the pH of the solutions. Cesium chloride, (CsCl), and cobalt chloride, ($CoCl_2$), purchased from Merck, (Germany). For all experiments, double-distilled water used for the preparation of solutions.

Preparation of nano- ZrO_2 [25]

Nano-sized ZrO_2 is prepared by the gelation method using Zirconium n-propoxide in presence of glacial acetic acid and isopropyl alcohol as well as water. 10 mol of isopropyl alcohol and 0.5 mol of water as well as stabilizer (8% MgO for 1 mol Zirconium n-propoxide) added gradually to 1 mol Zirconium n-propoxide with glacial acetic acid. The overall mixture stirred for 10 min. The gel appeared by adding isopropyl alcohol and water.

Sorbent preparation (CTS- ZrO_2) composites

CTS- ZrO_2 composites prepared by direct mixing method of the dried ZrO_2 nanoparticles to chitosan solution. 20 ml of ethanol, 30 ml of deionised water, and 1 ml of 1 M HCl were added to dry ZrO_2 . The whole mixture was stirred for 30 min using magnetic stirrer. ZrO_2 solution slowly added drop wisely to the previously prepared chitosan solution (chitosan dissolved in 200 ml of 2% acetic acid). The mixture treated ultrasonically for 10 min then stirred for a day. The prepared samples dried at 60 °C for 48 h then ground and stored for further use. Three different compositions of CTS- ZrO_2 composites prepared according to the following Table 1.

Instruments

The morphology of the particles recorded by (SEM, FEI Quanta FEG-250, and EDX). The molecular vibration of the characteristic function group of the adsorbents assigned by KBr pellet technique on a Perkin Elmer 1600 FTIR Spectrophotometer in wave number range 600–4000 cm^{-1} . The thermal stability of the adsorbents is achieved by Shimadzu DT- 60, Japan. The Samples exposed to temperature up to 800 °C with a heating rate of 20 °C min^{-1} in the presence of nitrogen atmosphere to avoid thermal oxidation of the powder samples. The crystal phases and nature of the adsorbents if amorphous or crystalline is recognized by X-ray diffraction (XRD) in a Philips X'PERT multipurpose X-ray diffractometer with copper emission lines. The particle size of the particles is measured by Zetasizer Nano-Zs, MALVERN (UK).

The concentration of Cs (I) and Co (II) measured with the aid of atomic absorption spectrophotometer (Buck Scientific, VGP 210).

Adsorption studies:

Adsorption studies were carried out onto CTS- ZrO_2 composites. Effect of pH, variation of contact time (10–120 min), changing initial concentration (100–500 $mg L^{-1}$) and influence of sorbent weight was studied to determine the best conditions for adsorption reaction. 0.05 g of the adsorbent contacted with 50 ml of the adsorbate solution and after equilibrium time; samples were filtered and separated from the solution using a well capped

Table 1 Compositions of the prepared samples in 100 ml solution

Sample	Composition ZrO_2 : chitosan	Dried- ZrO_2 (g)	Chitosan (g)
CTS- ZrO_2 -1	1:2	2	4
CTS- ZrO_2 -2	1:1	3	3
CTS- ZrO_2 -3	2:1	4	2

centrifuge tubes. The residual metal ion concentrations in the filtrate defined. The pH values regulated using 0.1 M HCl and 0.1 M NaOH solutions. The adsorption efficiency and adsorbed amount determined using Eqs. (1) and (2), respectively.

$$\text{Adsorption-efficiency (\%)} = \left(\frac{C_0 - C_e}{C_0} \right) \times 100 \quad (1)$$

Adsorbed amount q ($\text{mg}\cdot\text{g}^{-1}$) calculated using Eq. (2):

$$q = \text{Adsorption-efficiency} \times C_0 \times \frac{V}{m} \quad (2)$$

Where q , is the adsorbed amount ($\text{mg}\cdot\text{g}^{-1}$). C_0 and C_e are the initial and equilibrium concentrations of the Cs (I) and Co (II). m is the mass of the adsorbent (g) and V volume of solution (L).

Kinetic modelling:

The mechanism of the adsorption reaction could be predicted by applying kinetic modelling. Three kinetics models applied through this study; Pseudo 1st order, pseudo 2nd order and intra-particle diffusion model.

Pseudo 1st order & pseudo 2nd order models:

The pseudo 1st order equation given by equation (3) [26]

$$\text{Log}(q_e - q_t) = \text{log } q_e - \frac{k_1}{2.303} t \quad (3)$$

Where q_e and q_t are the adsorbed amounts of Cs (I) or Co (II); ($\text{mg}\cdot\text{g}^{-1}$) at equilibrium time and at any time t , respectively; k_1 (min^{-1}) is the 1st order rate constant.

The pseudo 2nd order described by the equation (4) [27]

$$\frac{t}{q_t} = \frac{1}{k_2 q_e^2} + \frac{1}{q_e} t \quad (4)$$

Where k_2 ($\text{g}\cdot\text{mg}^{-1} \text{min}^{-1}$) is the 2nd order rate constant.

Intra- particle diffusion model:

The intra-particle diffusion model applied using Eq. (5) [28]

$$q_t = K_{id} t^{0.5} + C \quad (5)$$

Where k_{id} is the intra-particle diffusion rate constant $\text{mg}\cdot\text{g}^{-1} \text{min}^{-1/2}$ and C is the intercept

Isotherm modeling:

Three isotherm models applied through this study; Langmuir [29], Freundlich [30], and Dubinin-Radushkevich model [31].

Langmuir model:

Equation (6) applied to examine Langmuir isotherm model fitting.

$$\frac{C_e}{q_t} = \frac{1}{bQ_0} + \frac{1}{Q_0} C_e \quad (6)$$

Where Q_0 is the monolayer adsorption capacity ($\text{mg}\cdot\text{g}^{-1}$), b is the constant related to the free energy of adsorption ($b \propto e^{-\Delta G/RT}$) and C_e is the equilibrium metal ion concentration. Also, the separation factor (R_L) is determined from the Langmuir model using the following Eq. (7).

$$R_L = \frac{1}{1 + bC_0} \quad (7)$$

where C_0 , $\text{mg}\cdot\text{L}^{-1}$, represents the initial concentration of Cs (I) and Co (II) ions. The values R_L used to show the type of the adsorption isotherm; irreversible ($R_L = 0$), favorable ($0 < R_L < 1$), linear ($R_L = 1$), or unfavourable ($R_L > 1$).

The Gibbs free energy of adsorption, ΔG ($\text{kJ}\cdot\text{mol}^{-1}$) can also evaluate from the characteristics b , Q according to the expression (8, 9):

$$K_C = bQ_0 \quad (8)$$

$$\Delta G = -2.303RT \log K_C \quad (9)$$

Where R is universal gas constant $8.314 \text{ J}\cdot\text{mol}^{-1} \text{ K}^{-1}$, and T is absolute temperature. The values of other thermodynamic parameters such as ΔH° ($\text{kJ}\cdot\text{mol}^{-1}$) (and ΔS° ($\text{J}\cdot\text{mol}^{-1} \text{ K}^{-1}$) calculated from the slope and intercept of the line relation between $\ln K_C$ and $1/T$ in Eq. (10), (11).

$$\Delta G = \Delta H - T\Delta S \quad (10)$$

$$\log K_C = \frac{\Delta S^\circ}{2.303R} - \frac{\Delta H^\circ}{2.303RT} \quad (11)$$

Freundlich model

Freundlich model represented by Liner Eq. (12).

$$\log q_e = \log K_f + \frac{1}{n} \log C_e \quad (12)$$

Where, K_f is Freundlich constant and n related to adsorption capacity and intensity.

Dubinin-Radushkevich model [31]:

It is an empirical adsorption model assuming the adsorption occurs on heterogeneous surface by pore filling mechanism.

It usually used to differentiate between physical and chemical adsorption. The linear equation of this model given by Eq. (13).

$$\ln q_e = \ln q_m - \beta \varepsilon^2 \quad (13)$$

Where q_m is monolayer capacity, β is a constant obtained by plotting relation between $\ln q_e$ and ε^2 and related to apparent adsorption energy $E = \frac{1}{\sqrt{2\beta}}$, ε is Polanyi potential and can be calculated from Eq. (14),

$$\varepsilon = RT \ln \left(1 + \frac{1}{C_e} \right) \quad (14)$$

Where R is a gas constant equals $8.3 \text{ J.K}^{-1}.\text{mol}^{-1}$, T is temperature degree (K).

Desorption study

CTS-ZrO₂-1 loaded by Cs (I) or Co (II) desorbed using HNO₃ as a desorbing solution. Different concentrations of HNO₃ (0.1, 0.3, 0.5 and 1 molL⁻¹) shaken with 0.05 g of CTS-ZrO₂-1 composite for 2 h. The mixture was filtrate to isolate the CTS-ZrO₂-1 composite from the liquid phase, and then Cs (I) or Co (II) ions concentration measured. The desorption efficiency % calculated using Eq. (15):

$$\text{Desorption \%} = \frac{C_{aq}}{C_s} \% \quad (15)$$

Where C_{aq} is that the concentration of Cs (I) or Co (II) within the aqueous phase, C_s is that the concentration of Cs (I) or Co (II) within the CTS-ZrO₂-1 composite.

Result and discussion:

Characterization of the prepared materials:

Point of zero charge (pH_{pzc}):

The point at which the charge of sorbent surface equal zero is known as point of zero charge (pzc). The pH_{pzc} plays a key role in the surface science as it demonstrates the material's efficiency to adsorb contaminated ions from various media. Below pH_{pzc}, the charge of the surface is positive, and over it the charge of surface is negative. The low value of point of zero charge signalizes that the used sample is an efficient material for adsorption process because of the surface of the material has a negative charge at a vast of pH range. Therefore, the surface successfully attracts the cations over a wide pH range.

pH_{pzc} of the composites surface estimated by batch technique. 0.1 g of the sorbent added to glass bottles with 10 ml

of 0.1 M NaCl and the solution shaken over night at 25 °C at different initial pH values. The final pH of the solution measured. The pH_{pzc} record when the final pH equals the initial pH [24, 32].

Figure 1 exhibits the relation between the initial pH, and ΔpH (The difference between the final and initial pH). The pH_{pzc} of CTS-ZrO₂-1, CTS-ZrO₂-2 and CTS-ZrO₂-3 are found to be 5.8, 6.2 and 6.8. These results coincides by authors [24]. Thus, CTS-ZrO₂-1 expected to have higher effective adsorption efficiency.

Fourier transforms infrared analysis:

FT-IR spectral analysis used to investigate the characteristic functional groups as well as bonding interaction in CTS-ZrO₂ composites. The FT-IR spectra of CTS-ZrO₂ composites are shown in Fig. 2. The three CTS-ZrO₂ composites spectra have the same characteristics bands but its intensity differs in the order CTS-ZrO₂ -1 > CTS-ZrO₂ -2 > CTS-ZrO₂ -3. In these three spectra, a broad band appears at 3400 cm⁻¹ and 1632 cm⁻¹ due to the bending and stretching vibrations of the O–H bond of adsorbed water molecules [33] and N–H stretching bond [34]. The absorption bands around 2925 cm⁻¹ attributed to C-H symmetric stretching. The absorption band at 1300 assigned to C-N stretching amide group. The bands around 1451 and 1416 cm⁻¹ belonged to CH₂ bending and CH₃ symmetrical deformations, respectively. The absorption band at 1157 cm⁻¹ assigned to asymmetric stretching of the C–O–C bridge [34]. The bands in range 895- 418 cm⁻¹ ascribed to ZrO₂ powder [33].

Figure 2d investigates the peaks corresponding to ZrO₂. A sharp observed peak in the range 474–601 cm⁻¹ attributed to vibration mode of ZrO₃²⁻ group [35]. The prominent two peak of 1330 and 1629 cm⁻¹ region corresponds to O–H vibration band of hygroscopic adsorbed H₂O [35].

However, Fig. 2e represents the corresponding vibrations bands of CTS. A strong band in the region 3288–3361 cm⁻¹ corresponds to N–H and O–H stretching, as well as the intermolecular hydrogen bonds. The absorption bands at around 2977 and 2876 cm⁻¹ can be attributed to C-H symmetric and asymmetric stretching, respectively. A band at 1648 cm⁻¹ corresponds to the N–H bending of the primary amine [33]. The CH₂ bending and CH₃ symmetrical deformations were confirmed by the presence of bands at around 1376 and 1310 cm⁻¹, respectively. The bands at 1066 and 1022 cm⁻¹ correspond to C-O stretching.

X-ray diffraction

X-ray diffraction (XRD) is one of the most important analysis methods for phase structure identification. The broad peaks suggest amorphous nature of the CTS-ZrO₂ composites. XRD patterns of CTS-ZrO₂ composites are shown

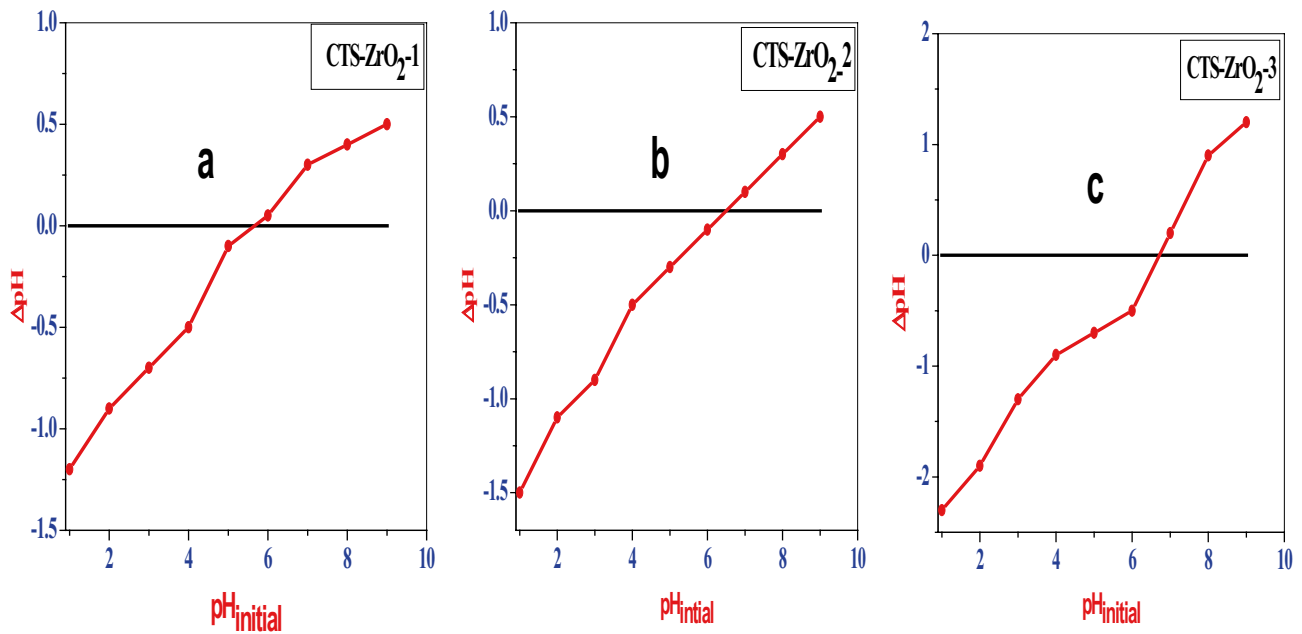


Fig. 1 Point of zero charge of different composites a- CTS-ZrO₂-1 b- CTS-ZrO₂-2 and c- CTS-ZrO₂-3

in Fig. 3 The broad peak at $2\theta \sim 30^\circ$, corresponding to the amorphous crystal phase of ZrO₂ [36]. The broad amorphous peaks are due to hydrogen bonding between Chitosan and ZrO₂ matrices which disrupts the inter chain hydrogen bonding in the Chitosan host polymer and thus results in less crystalline [37].

For dried ZrO₂ has amorphous structure due to existence of O–H group [35]. While the the diffract gram of chitosan in Fig. 3e shows to crystalline peaks at 10° and

20° which disappear in the CTS-ZrO₂ composite for cross linking chitosan and show boarder amorphous structure due to presence of water [38].

Particle size distribution

The distribution of particle size revealed in Fig. 4. The particle size in ZrO₂ is fine and range in between 140–220 nm.

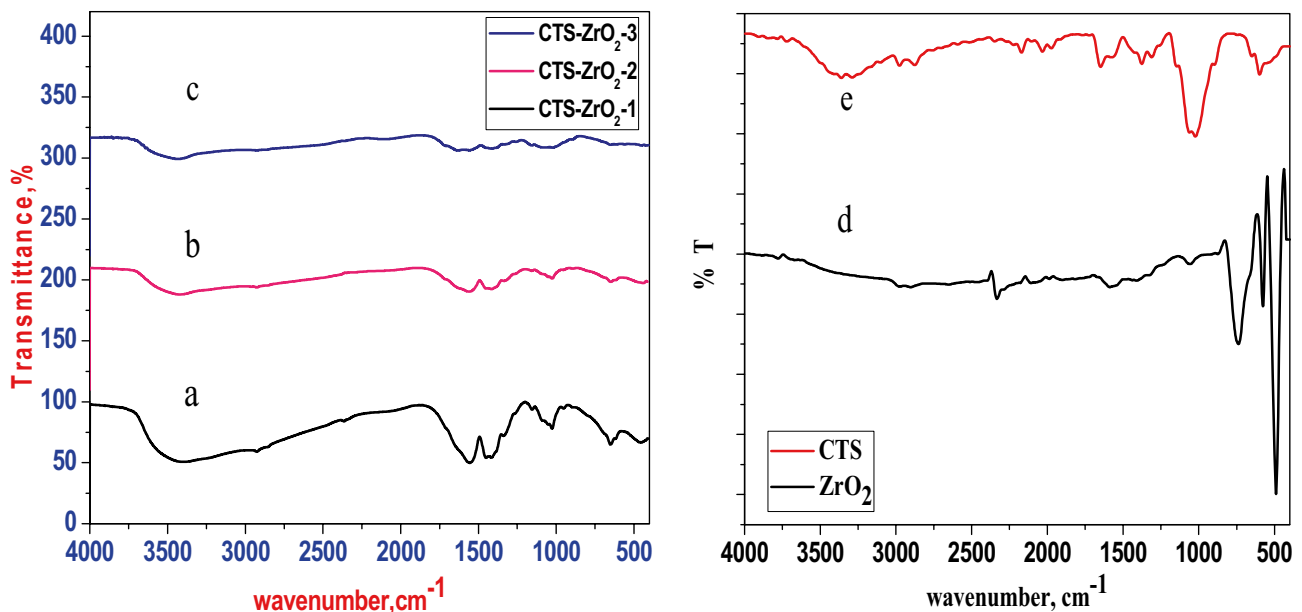


Fig. 2 FT-IR spectrum of a- CTS-ZrO₂-1 composite -1 b- CTS-ZrO₂-2 composites c- CTS-ZrO₂-3 composite d- ZrO₂ e- CTS

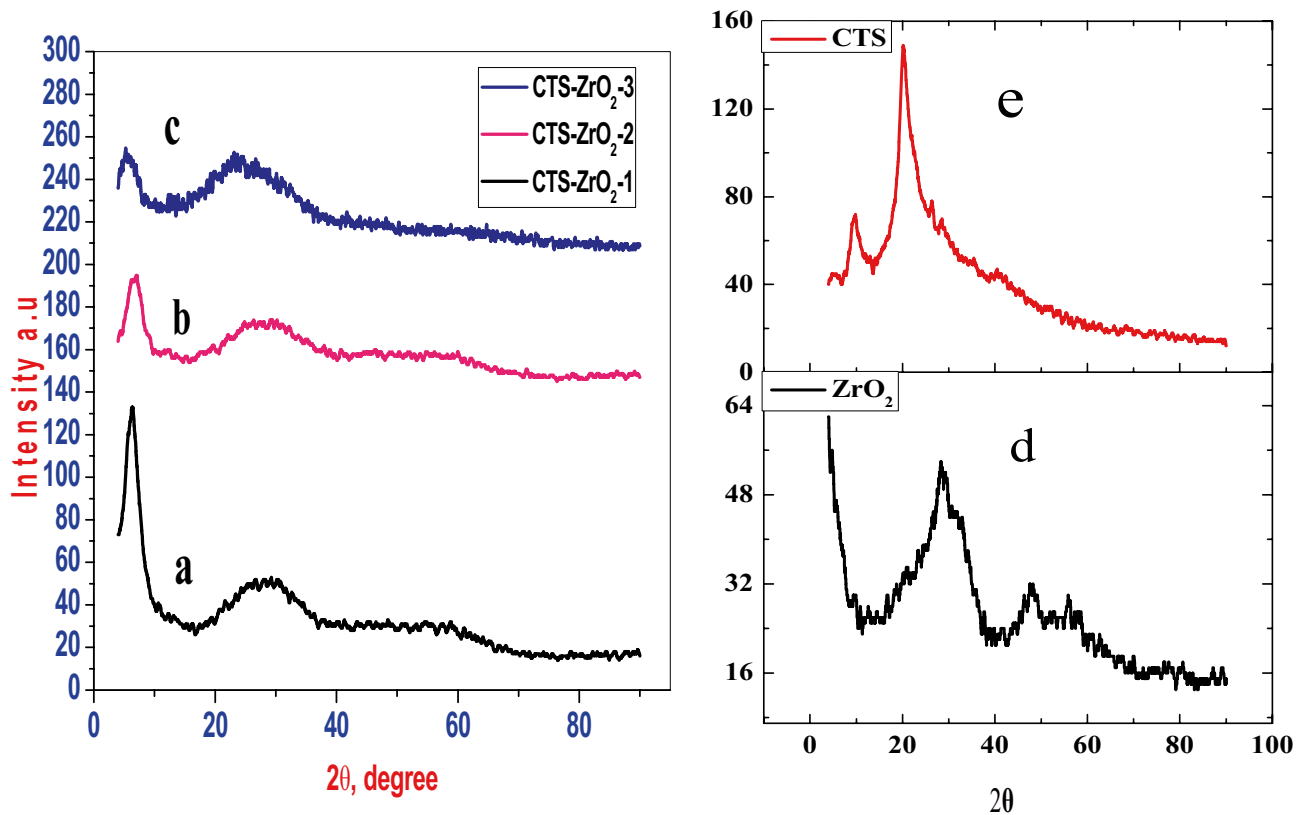


Fig. 3 X-ray diffraction of a- CTS-ZrO₂-1 composite -1 b- CTS-ZrO₂-2 composites c- CTS-ZrO₂-3 composite d- ZrO₂ e- CTS

After adding ZrO₂ to chitosan in CTS-ZrO₂-1 composite, the particle size increase and range from 250–850 nm due to bulky size of the polymer and/or agglomeration of ZrO₂ on the surface of chitosan.

SEM-analysis

SEM analysis investigated the morphology of the CTS-ZrO₂ composites. ZrO₂ scattered on Chitosan due to its wide surface in Fig. 5. The CTS-ZrO₂ composites have irregular agglomerated particles [39]. The surface of the composites are rough. The roughness of the surface and the particle size increase as the incorporation percent ratio of ZrO₂ increases.

Thermal analysis

TGA-DTA analysis is an important technique, refers to the thermal stability of CTS-ZrO₂ composites. Figure 6

represents TGA-DTA for the three compositions of CTS-ZrO₂ composites.

All the three composites shows an endothermic peak at temperatures 143.3, 159.9 and 160.9 °C accompanied by weight loss 13.05, 12.8, 12.55% for CTS-ZrO₂-1, CTS-ZrO₂-2 and CTS-ZrO₂-3 composites, respectively. This endothermic peak is due to dehydration of hygroscopic and structural water.

For CTS-ZrO₂-1 in Fig. 6a, A sharp exothermic peak at 245 °C with weight loss 25.8% due to decomposition of organic chitosan polymer. Finally, 18% weight loss up to 600 °C because of the complete degradation of chitosan [40]. CTS-ZrO₂-2 and CTS-ZrO₂-3 have the same trend with weights loss started from 22.5% and 19.5%, respectively and ends with weight loss 15% and 11.5% for CTS-ZrO₂-2 and CTS-ZrO₂-3, respectively.

Thus, CTS-ZrO₂-1 shows a total 57.7% weight loss till 600 °C while CTS-ZrO₂-2 and CTS-ZrO₂-3 composites has 54.3 and 53.3% weight loss.

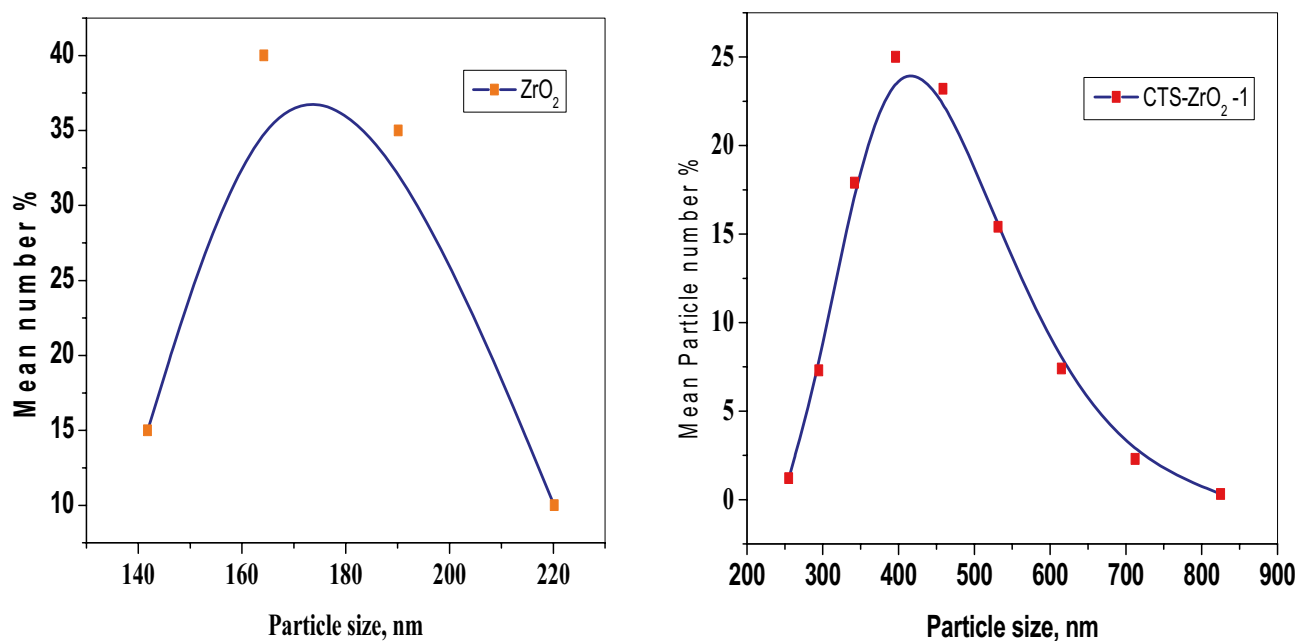


Fig. 4 Particle size distribution a) ZrO₂ b) CTS-ZrO₂-1 composites

Adsorption study:

The influence of pH

The pH values are considered one of the important parameters impact the adsorption process because of the pH value has a great influence on the interaction between the adsorbate and the adsorbent. The studying of impact of pH values on the adsorption process of Co (II) and Cs (I) needed batch study in pH range from 1 to 9 (Fig. 7) with metal ions concentrations 100 mgL⁻¹ and shaking time 24 h. As the pH increased, the removal efficiency of

studied ions increased. At high pH values, the charge of surface become negative, the interaction between the metal ions and the surface increase and therefore, the removal of the ions increases. At low pH, the surface charge is positive, the competition between [H]⁺ with studied ions increase, therefore the removal of cesium and cobalt ions decrease [41–43]. Figure 6 shows CTS-ZrO₂-1 has higher adsorbed amount compared to CTS-ZrO₂-2 & CTS-ZrO₂-3 in agreement with the zero point charge results.

The speciation diagram of Cs (I) and Co (II) ions at different pH values in aqueous solution, shown in Fig. 8 using Hydra/Medusa chemical equilibrium software [44].

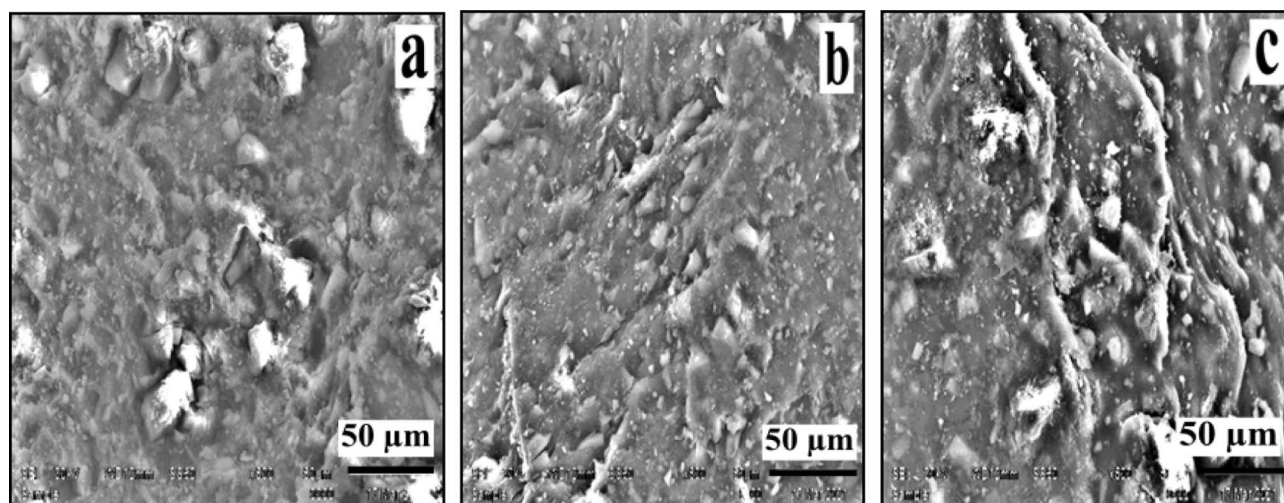


Fig. 5 SEM-analysis of a- CTS-ZrO₂-1 b- CTS-ZrO₂-2 and c- CTS-ZrO₂-3 composites

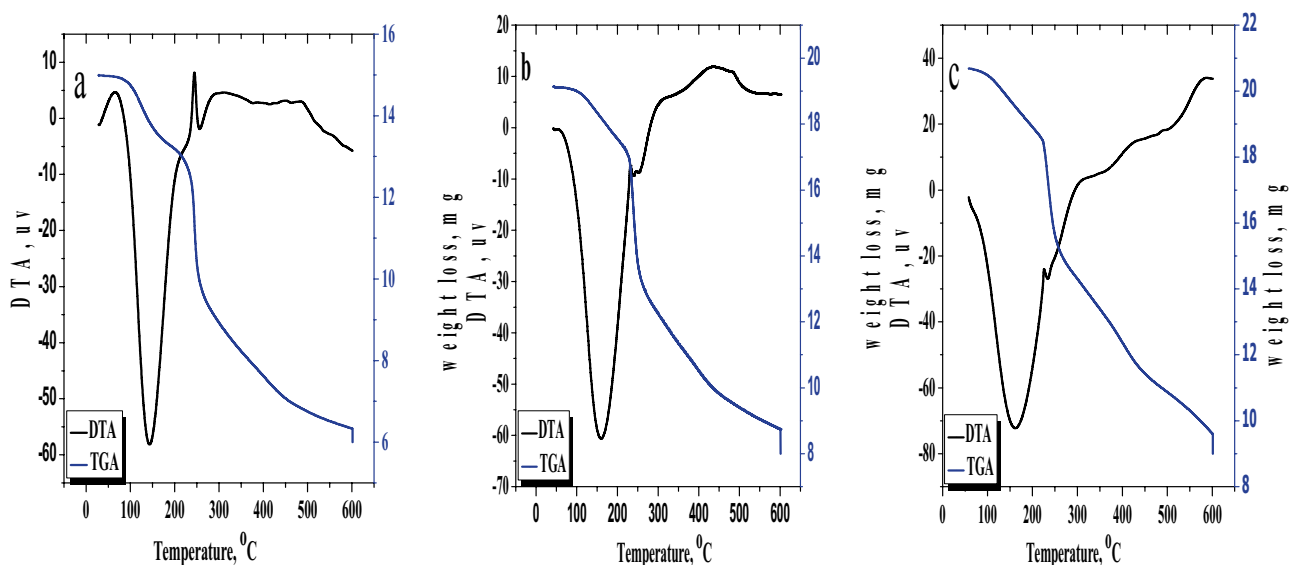


Fig. 6 TGA-DTA- analysis of a- CTS-ZrO₂-1 b- CTS-ZrO₂-2 and c- CTS-ZrO₂-3 composites

From Fig. 8a it is clear that the monovalent cesium Cs (I) is the dominant species at all pH ranges while the divalent species, Co (II), in Fig. 8b, is the dominant cobalt species at pH below 7. At pH > 7, the cobalt ion precipitated as Co (OH)₂.

The future adsorption studies executed at pH = 9 for Cs (I) and pH 6 for Co (II).

Effect of shaking time

The shaking time between the different ions and the adsorbent materials has great importance in treatment of

wastewater using the adsorption technique. Adsorption of Cs (I) and Co (II) ions studied utilizing CTS-ZrO₂-1 at three different temperatures (298, 308, and 318 K) and the adsorption equilibrium attained after 60 min, Fig. 9. The amount adsorbed increases by raising the temperature assigned to endothermic reaction.

Effect of organic complexation agent addition:

Figure 10 represents the efficiency of the adsorption process in presence of EDTA with different concentrations. As the concentration of EDTA increase, the amount adsorbed

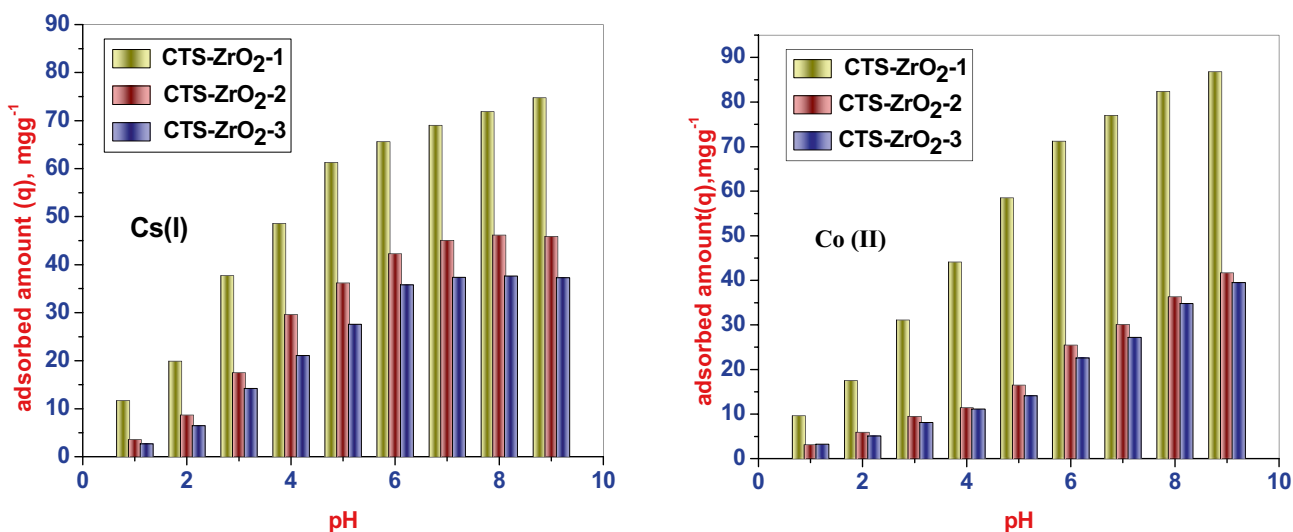


Fig. 7 The effect of pH on the adsorption of Cs (I) and Co (II) onto. CTS-ZrO₂-1, CTS-ZrO₂-2 and CTS-ZrO₂-3 composites

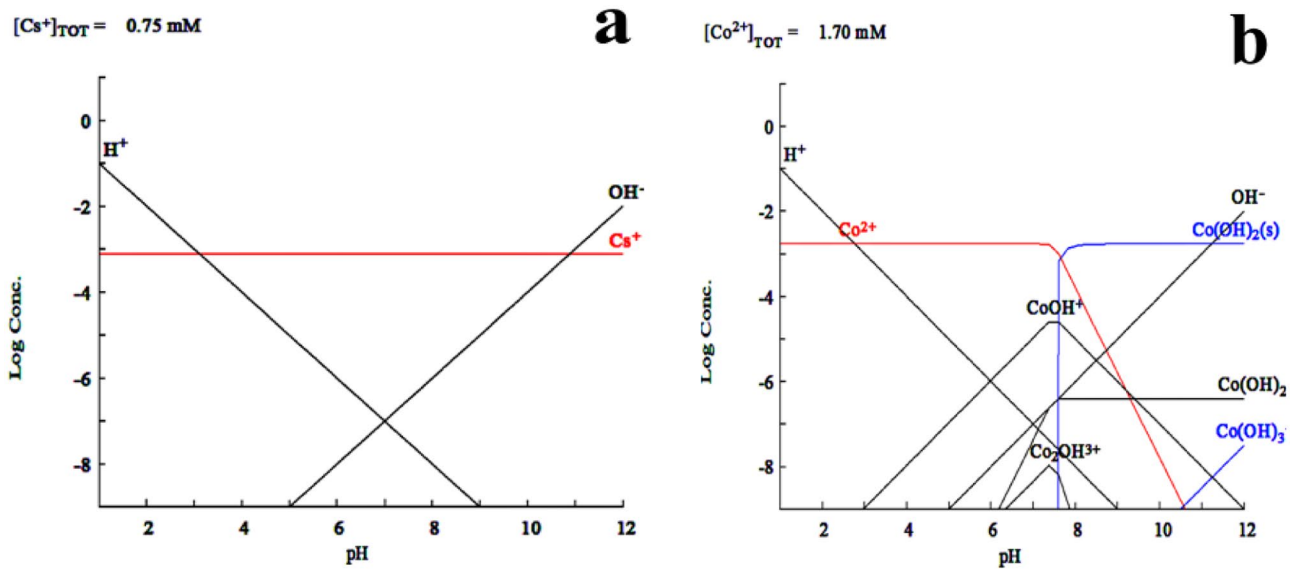


Fig. 8 Speciation of: a- Cesium and b- Cobalt ions at different pH and room temperature

decrease for both Cs (I) and Co (II). This belongs to the complexation tendency of these ions with EDTA and formation charged surface complexes between metal ion and

EDTA of and therefore, decrease concentration of Cs (I) and Co (II) ions available for adsorption on CTS-ZrO₂-1 composite [45].

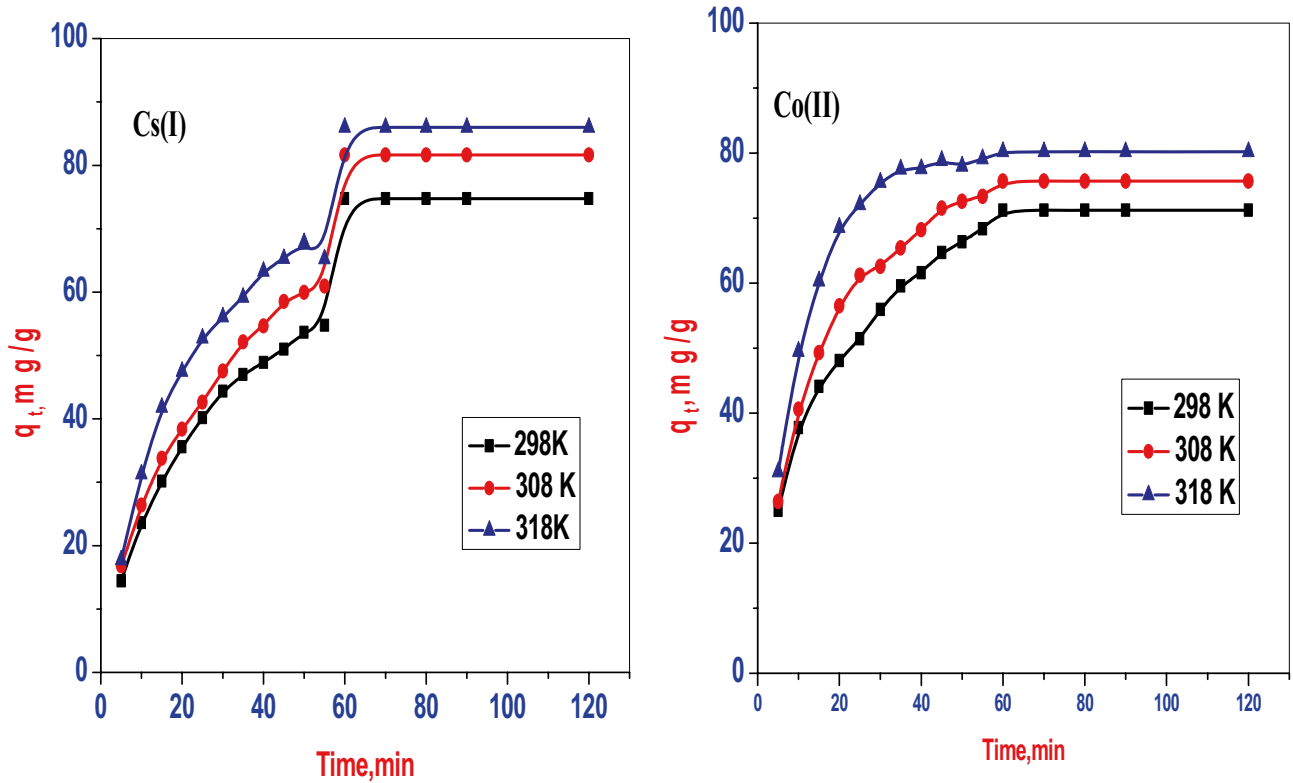


Fig. 9 Effect of shaking time on adsorption of Cs (I) and Co (II) onto CTS-ZrO₂-1 composite at different temperatures

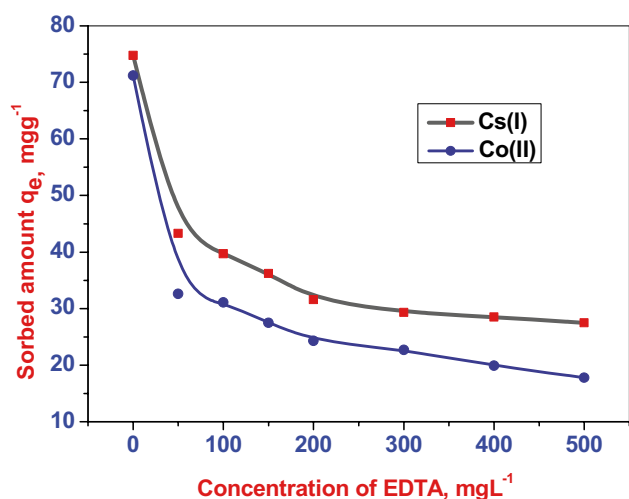


Fig. 10 Effect of EDTA on adsorption of Cs (I) and Co (II) onto CTS-ZrO₂-1 composite

Influence of concentration and temperature:

Figure 11 depicted the influence of concentration in the range 50–400 mgL⁻¹ on the adsorption of Cs (I) and Co (II) onto CTS-ZrO₂-1 composite. As the concentration increase, q_e will increase which attributed to mass transfer interaction [46] as the collision of the selected metal ions to CTS-ZrO₂-1 composite surface increase resulting in increase in the adsorption extent. The amounts adsorbed for Cs (I) onto CTS-ZrO₂-1 composite at 298, 308 and 318 K are 74.75, 81 and 84 mgg⁻¹, respectively and q_e for Co (II) are 71.81,

75.71 and 80.21 mgg⁻¹ at the same temperatures, respectively. The result clarified that the increasing temperature promoted the adsorption process and confirmed the endothermic character.

Adsorption kinetics mechanism

The kinetic models of the studied ions performed to explain the adsorption behaviour of CTS-ZrO₂-1 composite. The adsorption kinetic of studied ions from an aqueous solution was investigated using pseudo 1st order, pseudo 2nd order and intra particle diffusion.

For pseudo 1st order kinetic model, the straight line acquired using plot $\log(q_e - q_t)$ with time t , Fig. 12. The amount of ions adsorbed at equilibrium (q_e) and constant of model (k_1) calculated from intercept and the slope of this straight line. Table 2 clarifies the values of q_e and k_1 of each studied ions at different temperatures. The obtained linear relation can be suggesting the pseudo 1st order model regulate the adsorption reaction. Also, the values of calculated amount of the adsorbed ions at equilibrium $q_{e(cal)}$, must be in uniformity with values of experimental data $q_{e(exp)}$. Table 2 illustrated that the values $q_{e(cal)}$ are not suitable with experimental values for each ion. Thus, adsorption reaction mechanism of Cs (I) and Co (II) onto CTS-ZrO₂-1 composite is not follow pseudo 1st order model.

The linear plot of t/q_t against time t for each ion, is shown for 2nd pseudo order fitting in Fig. 12. The values of pseudo 2nd model parameters illustrated in Table 2. The linearity relationship between the t/q_t against time t and the high

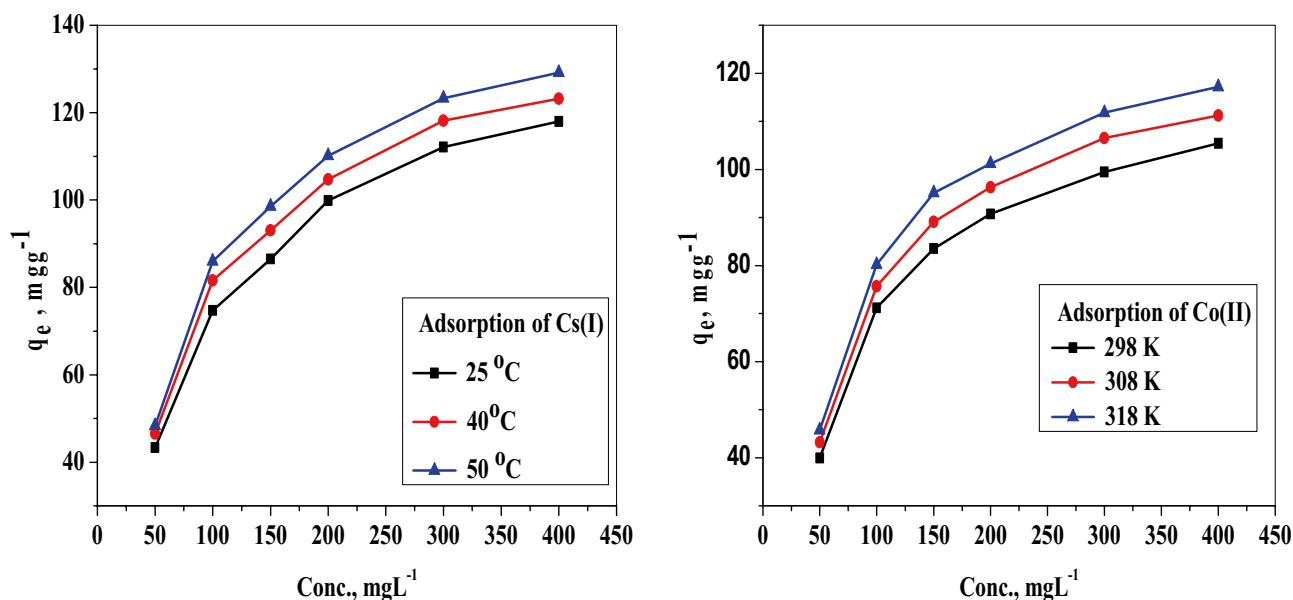


Fig. 11 Effect of concentration on adsorption of Cs (I) and Co (II) onto CTS-ZrO₂-1 composite at different temperatures

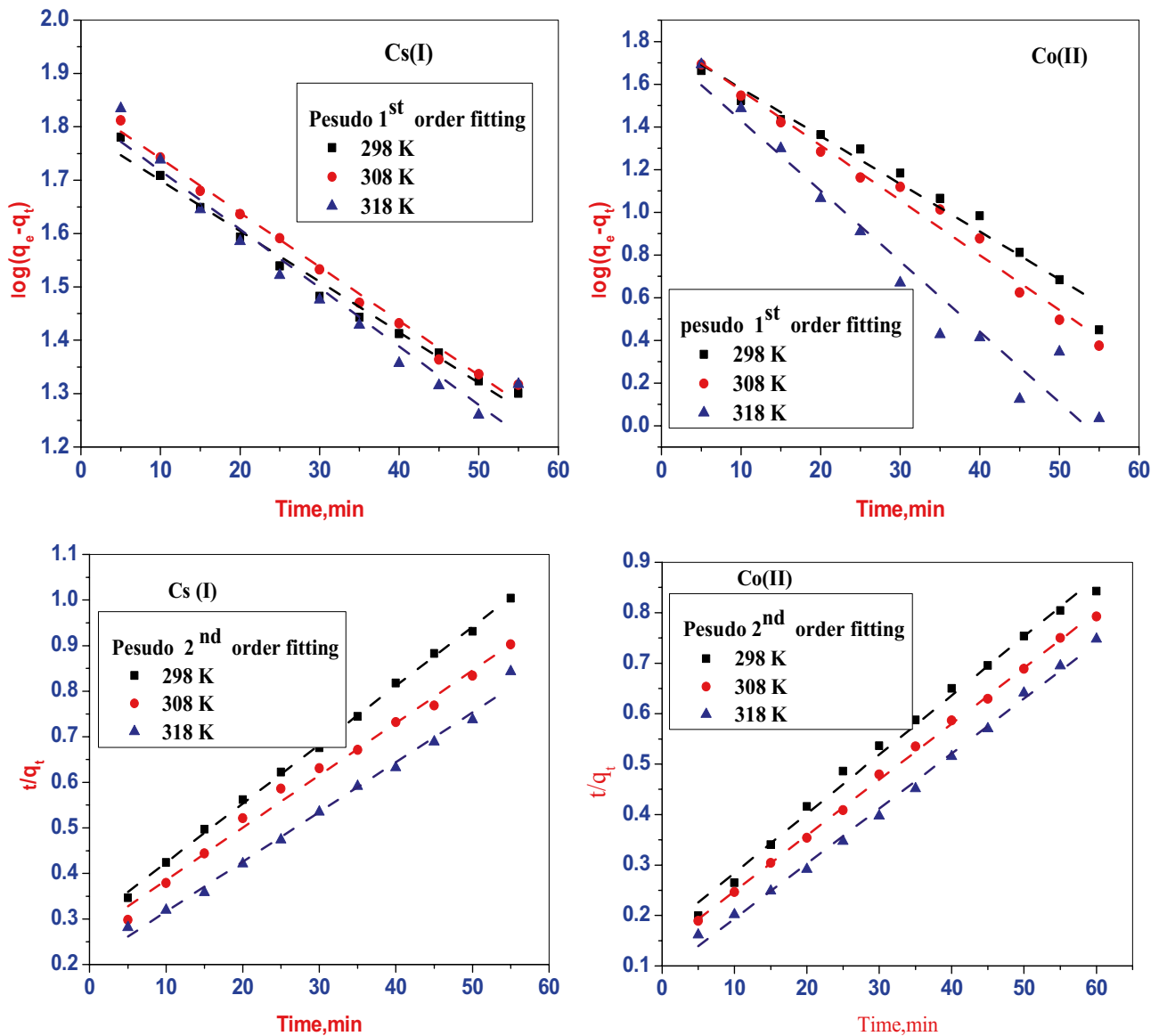


Fig. 12 Pseudo 1st order and pseudo 2nd order kinetic plots for the adsorption of Cs (I) and Co (II) ions onto CTS-ZrO₂-1 composite at different temperatures

values of R² clarify that the adsorption of Cs (I) and Co (II) ions follow the pseudo 2nd model as the calculated values of q_e are proper to the results of experimental values of q_{eexp}.

So, the pseudo 2nd order model is the dominant model, and adsorption process mechanism could be described by the chemical adsorption [47].

Table 2 The parameters of the pseudo 1st order and pseudo 2nd order kinetic models for Cs (I) and Co (II) ions adsorbed onto CTS-ZrO₂-1 composite at different temperatures

Metal ion	Temp., K	First-order kinetic parameters			Second-order kinetic parameters			q _e (exp), mg.g ⁻¹
		k ₁ , min ⁻¹	q _e (calc), mg.g ⁻¹	R ²	k ₂ , mg.g ⁻¹ .min ⁻¹	q _e (calc) mg.g ⁻¹	R ²	
Cs (I)	298	0.022	62.3	0.983	0.004	77.4	0.998	74.7
	308	0.023	67.1	0.991	0.005	86.6	0.991	81.6
	318	0.025	69.5	0.945	0.006	91.4	0.992	86.0
Co (II)	298	0.051	63.5	0.973	0.008	85.3	0.993	71.2
	308	0.059	67.1	0.984	0.009	86.2	0.999	75.7
	318	0.076	67.6	0.948	0.014	89.3	0.996	80.2

Figure 13 displays the intra-particle diffusion fitting for the adsorption of Cs (I) and Co (II) ions onto the surface of the prepared composite. It is obvious that this model for the adsorption of the Cs (I) and Co (II) ions occurred during multi stages. The first one characterizes the diffusion of the ions from the bulk of solution to the surface of the solid materials (from 1 to 50 min). The second stage (from 60 to 100 min) is the equilibrium saturation. The two stage of adsorption confirm the mechanism includes both film and intra-particle diffusion mechanism. Table 3 displays the different parameters acquired from the two parts of the plot [47].

Equilibrium isotherm

The adsorption isotherms for Cs (I) and Co (II) ions solutions onto CTS-ZrO₂-1 composite at different temperatures have been studied. Langmuir, Freundlich, and Dubinin-Radushkevich (DR) isotherm models were used to characterize the adsorption of both ions onto CTS-ZrO₂-1 composite.

The linear Langmuir relationship produced by plotting C_e versus C_e/q_e (Fig. 14) and from slope and intercept, the values of Q_0 and Langmuir constant (b) calculated and listed in Table 4. The values of Q_0 and b increase as the temperature increase. This can be owing to that increasing temperature lead to increase the available active sites and consequently, the adsorption efficiency increases. The results in Table 4 indicated that the adsorption of cesium and cobalt ions on the surface of CTS-ZrO₂-1 composite follows the Langmuir model over all concentration used. Also, R_L are ranged between zero and one; thus the types of the adsorption isotherms of each ion are favourable.

Table 3 Intra-particle diffusion parameters for the adsorption of Cs (I) and Co (II) ions onto CTS-ZrO₂-1 composite at different temperatures

Temperature (K)	Time rang (min)	K_{di} (mg.g ⁻¹ .min ^{-1/2})	R^2
Cs-298	1-50	11.20	0.97
	60-100	-	-
Cs-308	1-50	13.53	0.93
	60-100	-	-
Cs-318	1-50	23.50	0.98
	60-100	-	-
Co-298	1-50	12.7	0.91
	60-100	-	-
Co-308	1-50	15.45	0.96
	60-100	-	-
Co-318	1-50	24.10	0.93
	60-100	-	-

Freundlich isotherm is applied by plotting the linear relation between $\log C_e$ and $\log q_e$. K_f and $1/n$ determined from intercept and slope of the straight line, Fig. 14. The results in Table (4) exhibit that the $1/n < 1$ indicating that the adsorption of both ions onto CTS-ZrO₂-1 is concentration-dependent. R^2 for Freundlich were less than that R^2 of Langmuir model, so, the Langmuir model is more suitable for the adsorption mechanism of Cs (I) and Co (II) ions by CTS-ZrO₂-1 composite.

The linear relation between $\ln q_e$ and ε^2 was obtained for different studied ions as illustrated in Fig. 14. The DR isotherm model results listed in Table 5. E values of adsorption of ions at all studied temperature within the range 8 to 16 kJ.mol⁻¹; this ensures that the reaction follows chemisorption mechanism [48].

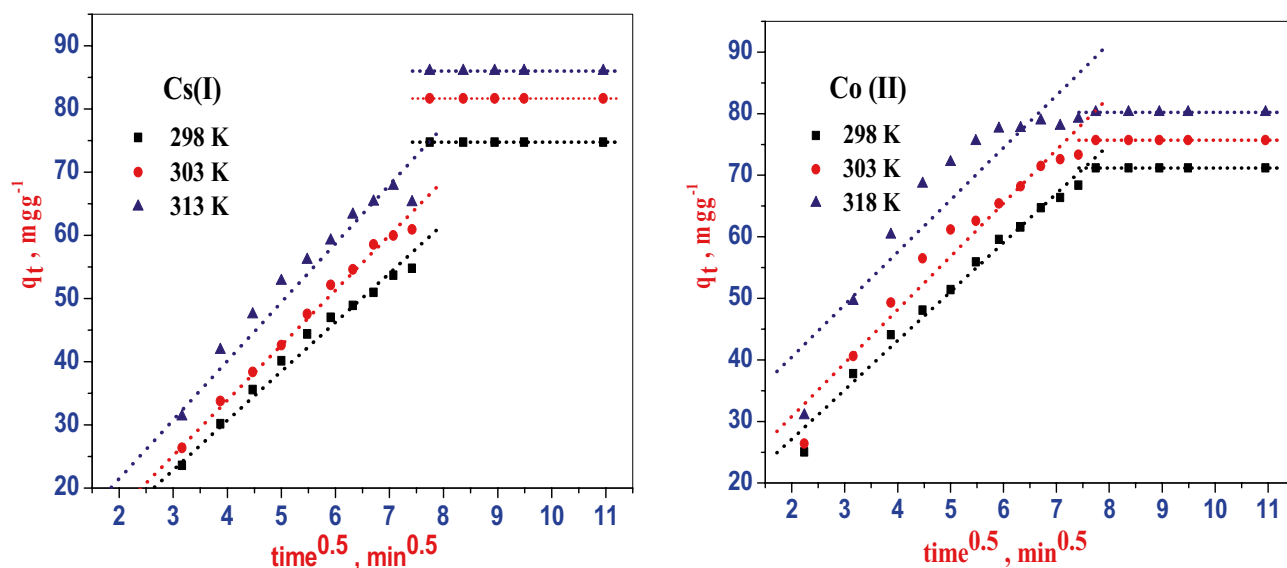


Fig. 13 Weber–Morris kinetic plots for the adsorption of Cs (I) and Co (II) ions onto CTS-ZrO₂-1 composite at different temperatures

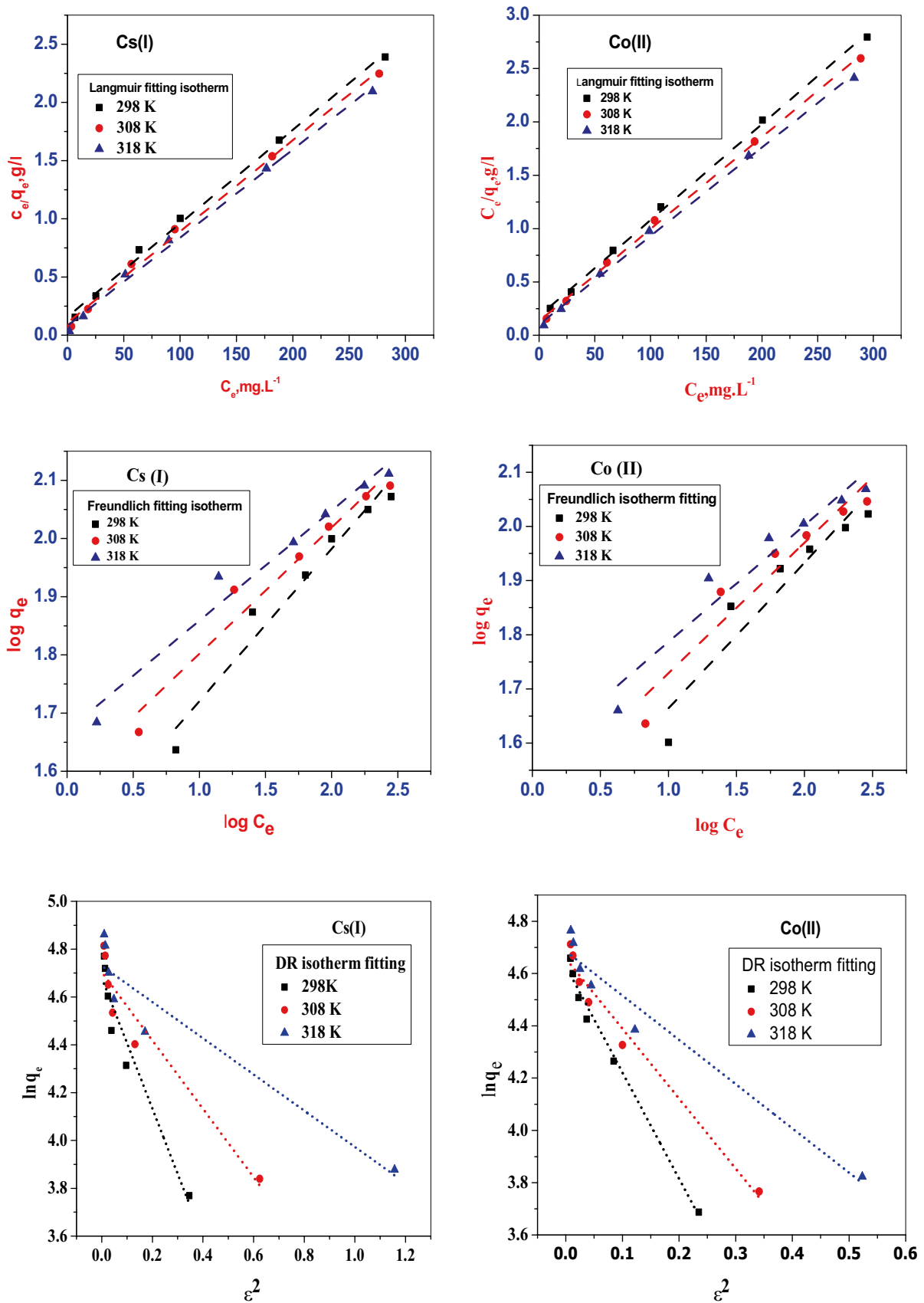


Fig. 14 Isotherm plots for the adsorption of Cs (I) and Co (II) ions onto CTS-ZrO₂-1 composite at different temperatures

Table 4 Langmuir and Freundlich isotherm coefficients for of Cs (I) and Co (II) ions the adsorption onto CTS-ZrO₂-1 composite

Metal ion	Temp., K	Langmuir coefficients				Freundlich coefficients			
		Q_0 mg.g ⁻¹	b , L.mg ⁻¹	R^2	R_L	n	K_f , mg.g ⁻¹	R^2	
Cs (I)	298	124.6	0.050	0.996	0.167	3.8	28.7	0.952	
	308	127.6	0.073	0.996	0.120	4.6	38.4	0.951	
	318	132.1	0.093	0.996	0.097	5.3	46.7	0.964	
Co (II)	298	111.1	0.049	0.998	0.169	3.7	24.8	0.882	
	308	115.9	0.064	0.998	0.135	4.1	30.7	0.907	
	318	120.5	0.082	0.998	0.109	4.6	37.3	0.921	

Table 5 DR isotherm coefficient of Co (II) and Cs (I) ions adsorbed onto CTS-ZrO₂-1 composite

Temp K	β , mol ² kj ⁻²		q_m , mmolg ⁻¹		R^2		E, kJ.mol ⁻¹	
	Cs (I)	Co (II)	Cs (I)	Co (II)	Cs (I)	Co (II)	Cs (I)	Co (II)
298	-0.023	-0.020	0.81	0.77	0.982	0.983	10.73	2.24
308	-0.021	-0.018	0.83	0.79	0.916	0.966	1.92	3.67
318	-0.020	-0.0175	0.852	0.81	0.959	0.979	2.21	4.33

Thermodynamic studies:

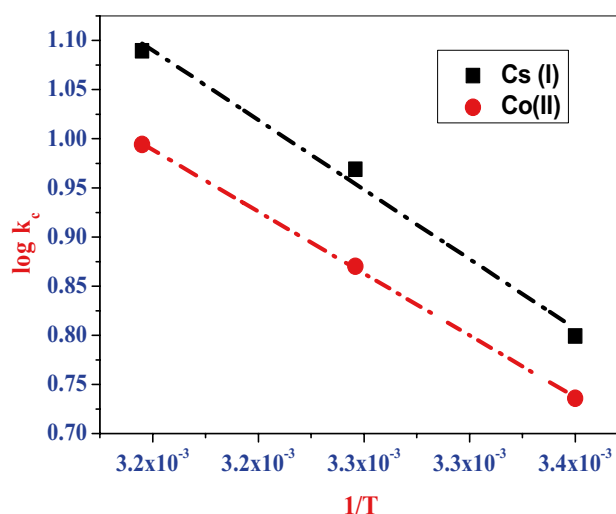
ΔH° and ΔS° could be determined from the slope and the intercept of the line plotted of $\log K_c$ against $1/T$ (Fig. 15) and illustrated in Table 6. $\Delta H^\circ > 0$ indicates the adsorption process is endothermic and $\Delta S^\circ > 0$ means the randomness at the composite /solution surface increase during the adsorption process. $\Delta G^\circ < 0$ indicates the adsorption process is spontaneous. As the temperature increase, the negativity of ΔG° as well as the degree of spontaneity of the process increase [49].

Desorption studies:

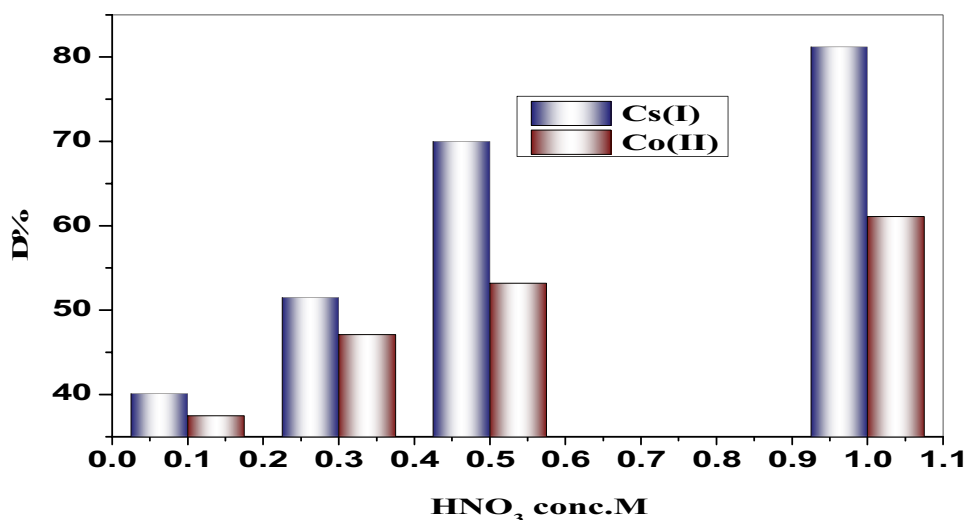
Desorption process can save cost and recycling hazardous waste. The more desorption percentage is the more efficient process and a remark or the good sorbent [50]. The desorption efficiency was studied (Fig. 16) for HNO₃ with various concentrations 0.1, 0.3, 0.5 and 1 molL⁻¹. 1 molL⁻¹ HNO₃ solution shows maximum desorption efficiency percent 81.2% and 61.1% for Cs (I) and Co (II), respectively. So, it's recommended to use 1 molL⁻¹ HNO₃ as an eluent for CTS-ZrO₂-1 composite desorption.

Comparison with other adsorbents

Table 7 includes the maximum adsorption capacity of CTS-ZrO₂-1 composite compared to that of other adsorbents for Cs (I) and Co(II). The comparison clarified that CTS-ZrO₂-1 composite could be used as an efficient adsorbent for Cs (I) and Co (II).

**Fig. 15** A plot against $\log K_c$ to $1/T$ for Cs (I) or Co (II) adsorption onto CTS-ZrO₂-1 composite**Table 6** Thermodynamic Coefficients for Cs (I) and Co (II) adsorption of metal ions onto CTS-ZrO₂-1 composite

Metal ions Temperature	ΔG° , kJmol ⁻¹			ΔH° , kJmol ⁻¹	ΔS° , Jmol ⁻¹ K ⁻¹
	298 K	313 K	333 K		
Cs (I)	-4.332	-5.911	-8.017	27.0475	105.30
Co (II)	-4.165	-5.589	-7.486	24.109	94.879

Fig. 16 Desorption of Cs (I) and Co (II) ions using HNO₃**Table 7** A comparison of the maximum adsorption capacity for Cs (I) and Co (II) ions with different adsorbents

Adsorbent materials	Adsorption capacity (mgg ⁻¹)		References
	Cs (I)	Co (II)	
Natural clinoptilolite	49.02	2.93	[51]
Myriophyllum spicatum	58.00	43.40	[52]
Graphite nanostructures	11.2	6.5	[53]
Chitosan–chloroacetic acid	193.1	NR	[54]
Brown seaweed	NR	20.6	[55]
Coal and chitosan	3.0	NR	[56]
Sheep wool	NR	15.08	[57]
Xanthate–modified magnetic chitosan	18.5	NR	[58]
CTS–ZrO ₂ -1 composite	124.6	111.1	This work

Conclusion

Three different Chitosan/ZrO₂ (CTS-ZrO₂) composites were successfully prepared by sol–gel method. Characterization of the CTS-ZrO₂ composites carried out through SEM, XRD, TGA/DTA, FT-IR and particle size distribution techniques. CTS-ZrO₂-1 with composition 1 (ZrO₂): 2(Chitosan) selected for adsorption of Cs (I) and Co (II) from aqueous solutions. The adsorption equilibrium was reached after about 60 min and pH optimized to be 9 for Cs (I) and 6 for Co (II). The results indicated that, pseudo 2nd order model is more regulated for the adsorption process. The adsorption process shows endothermic character. Langmuir model is more suitable for the reaction mechanism. The maximum adsorption capacities of Cs (I) and Co (II) onto CTS-ZrO₂-1 are 124.6 and 111.1 mgg⁻¹, respectively. Therefore, the prepared CTS-ZrO₂-1 is an efficient composite for adsorption of Cs (I) and Co (II) metal ions from aqueous solutions.

Author contributions All authors contributed to the study conception and design, Material preparation, data collection and analysis. All authors read and approved the final manuscript.

Funding The authors received no financial support for the research, authorship, and/or publication of this article.

Availability of data and materials All the data used for this work are publicly available.

Declarations

Ethical approval The authors confirm that the manuscript has been read and approved by all authors. The authors declare that this manuscript has not been published and not under consideration for publication elsewhere.

Consent to participate All of the authors consented to participate in the drafting of this manuscript.

Consent for publication All of the authors consent to publish this manuscript.

Research involving human participants and/or animals Not applicable.

Conflict of interest The authors declare that they have no conflict of interest.

References

1. Ambashta RD, Sillanpää MET (2012) Membrane purification in radioactive waste management: a short review. *J Environ Radioact* 105:76–84. <https://doi.org/10.1016/j.jenvrad.2011.12.002>
2. Horn S, Naidus E, Alper SL, Danziger J (2015) Cesium-associated hypokalemia successfully treated with amiloride. *Clin Kidney J* 8(3):335–338. <https://doi.org/10.1093/ckj/sfv017>
3. El-Kamash AM (2008) Evaluation of zeolite a for the sorptive removal of Cs⁺ and Sr²⁺ ions from aqueous solutions using batch

- and fixed bed column operations. *J Hazard Mater* 151:432–445. <https://doi.org/10.1016/j.jhazmat.2007.06.009>
4. Jia F, Wang J (2017) Separation of cesium ions from aqueous solution by vacuum membrane distillation process. *Prog Nucl Energy* 98:293–300. <https://doi.org/10.1016/j.pnucene.2017.04.008>
 5. Zaman H, Sharif S, Kim D, Idris M, Suhaimi MA, Tumurkhuyag Z (2017) Machinability of Cobalt-based and Cobalt Chromium Molybdenum Alloys - A Review. *Procedia Manufacturing* 11:563–570. <https://doi.org/10.1016/j.promfg.2017.07.150>
 6. Ivanets AI, Shashkova IL, Kitikova NV, Drozdova NV (2014) Extraction of Co (II) ions from aqueous solutions with thermally activated dolomite. *Russ J Appl Chem* 87:270–275. <https://doi.org/10.1134/S10663622140501295>
 7. Abdel-Rahman RO, El-Kamash AM, Ali HF, Hong YT (2011) Overview on recent trends and developments in radioactive liquid waste treatment. Part 1: sorption/ion exchange technique. *Int J Environ Eng Sci* 2:1–16
 8. Narbutt J, Bilewicz A, Bartoś B (1994) Composite ion exchangers. Prospective nuclear applications. *J Radioanal Nucl Chem* 183:27–32. <https://doi.org/10.1007/BF020431137>
 9. Bilewicz A, Narbutt J (2001) α -Crystalline polyantimonic acid: an adsorbent for radio strontium, and a potential primary barrier in waste repositories. *Radiochim Acta* 89:783–784. <https://doi.org/10.1524/ract.2001.89.11-12.7838>
 10. Chon K, Kim SJ, Moon J, Cho J (2012) Combined coagulation disk filtration process as a pre-treatment of ultrafiltration and reverse osmosis membrane for wastewater reclamation: an autopsy study of a pilot plant. *Water Res* 46(6):1803–1816. <https://doi.org/10.1016/j.watres.2011.12.0629>
 11. Montaña M, Camacho A, Serrano I, Devesa R, Matia L, Vallés I (2013) Removal of radionuclides in drinking water by membrane treatment using ultrafiltration, reverse osmosis and electrodialysis reversal. *J Environ Radioact* 125:86–92. <https://doi.org/10.1016/j.jenvrad.2013.01.010>
 12. Dakrouy GA, Abo-Zahra ShF, Hassan HS (2020) Utilization of olive pomace in nano MgO modification for sorption of Ni(II) and Cu(II) metal ions from aqueous solutions. *Arab J Chem* 13(8):6510–6522. <https://doi.org/10.1016/j.arabjc.2020.06.008>
 13. Wan Ngah WS, Teong LC, Hanafiah MAKM (2011) Adsorption of dyes and heavy metal ions by chitosan composites: A review. *Carbohydr Polym* 83:1446–1456
 14. Madill EAW, Garcia-Valdez O, Champagne P, Cunningham MF (2017) CO₂-responsive graft modified chitosan for heavy metal (nickel) recovery. *Polymers* 9(9):394. <https://doi.org/10.3390/polym9090394>
 15. Yazdani MR, Bhatnagar A, Vahala R (2017) Synthesis, characterization and exploitation of nano-TiO₂/feldspar embedded chitosan beads towards UV-assisted adsorptive abatement of aqueous arsenic (As). *Chem Eng J* 316:370–382. <https://doi.org/10.1016/j.cej.2017.01.121>
 16. Prabhu SM, Meenakshi S (2015) A dendrimer-like hyper branched chitosan beads toward fluoride adsorption from water. *Int J Biol Macromol* 78:280–286. <https://doi.org/10.1016/j.ijbiomac.2015.04.002>
 17. Yazdani M, Bahrami H, Arami M (2014) Feldspar/titanium dioxide/chitosan as a biophotocatalyst hybrid for the removal of organic dyes from aquatic phases. *J Appl Polym Sci* 131(10):40247–40256. <https://doi.org/10.1002/app.40247>
 18. Mahaninia MH, Wilson LD (2016) Cross-linked chitosan beads for phosphate removal from aqueous solution. *J Appl Polym Sci* 2:133. <https://doi.org/10.1002/app.42949>
 19. Cao J, Cao H, Zhu Y, Wang S, Qian D, Chen G, Sun M, Huang W (2017) Rapid and effective removal of Cu²⁺ from aqueous solution using novel chitosan and laponite-based nanocomposite as adsorbent. *Polymers* 9(1):5. <https://doi.org/10.3390/polym9010005>
 20. Wang X, Du Y, Liu H (2004) Preparation, characterization and antimicrobial activity of chitosan-Zn complex. *Carbohydr Polym* 56:21–26. <https://doi.org/10.1016/j.carbpol.2003.11.007>
 21. Yamani JS, Lounsbury AW, Zimmerman JB (2016) Towards a selective adsorbent for arsenate and selenite in the presence of phosphate: Assessment of adsorption efficiency, mechanism, and binary separation factors of the chitosan-copper complex. *Water Res* 1(88):889–896. <https://doi.org/10.1016/j.watres.2015.11.017>
 22. Kljajević L, Matović B, Radosavljević-Mihajlović A, M. Rosić M, Bosković S, Devečerskić A, (2011) Preparation of ZrO₂ and ZrO₂/SiC powders by carbothermal reduction of ZrSiO₄. *J Alloy Compd* 509(5):2203–2215. <https://doi.org/10.1016/j.jallcom.2010.11.002>
 23. Liu HL, Sun XF, Yin CQ, Hu C (2008) Removal of phosphate by mesoporous ZrO₂. *J Hazard Mater* 151(2–3):616–622. <https://doi.org/10.1016/j.jhazmat.2007.06.033>
 24. Jiang H, Chen P, Luo Sh, Tu X, Cao Q, Shu M (2013) Synthesis of novel nanocomposite Fe₃O₄/ZrO₂/chitosan and its application for removal of nitrate and phosphate. *Appl Surf Sci* 284:942–949. <https://doi.org/10.1016/j.apsusc.2013.04.013>
 25. Gehan AS (2003) Characterization of metal oxides extracted from different precursors and their application in nuclear technology. Ain Shams University Cairo, Egypt, Ph.D Faculty of Science
 26. Lagergren S (1898) About the theory of so-called adsorption of soluble substance. *Kungliga Svenska Vetenskaps-Akademiens Handlingar* 24:1–39
 27. McKay G, Ho YS (1999) Pseudo-second order model for sorption processes. *Process Biochem* 34:451–465
 28. Weber WT, Morris JC (1963) Kinetics of adsorption on carbon from solution. *J Sanit Eng Div Am Soc Civ Eng* 89:31–60
 29. Langmuir I (1918) The adsorption of gases on plane surfaces of glass, mica and platinum. *J Am Chem Soc* 40(9):1361–1403. <https://doi.org/10.1021/ja02242a004>
 30. Weidner E, Ciesielczyk F (2019) Removal of hazardous oxyanions from the environment using metal-oxide-based materials. *Materials* 12(6):927. <https://doi.org/10.3390/ma12060927>
 31. Dubinin MM (1960) The potential theory of adsorption of gases and vapors for adsorbents with energetically non-uniform surface. *Chem Rev* 60:235–266. <https://doi.org/10.1021/cr60204a006>
 32. Hassan HS, Attia LA, Dakrouy GA (2020) Exploration of the parameters affecting the radioactive europium removal from aqueous solutions by activated carbon-epoxy composite. *Appl Radiat Isot* 164:109278. <https://doi.org/10.1016/j.apradiso.2020.109278>
 33. Queiroz M, Melo K, Sabry D, Sasaki G, Rocha H (2014) Does the Use of Chitosan Contribute to Oxalate Kidney Stone Formation? *Marine Drugs* 13(1):141–158. <http://doi.org/10.3390/md13010141>
 34. Rao TN, Hussain I, Lee JE, Kumar A, Koo BH (2019) Enhanced Thermal Properties of Zirconia Nanoparticles and Chitosan-Based Intumescent Flame Retardant Coatings. *Appl Sci* 9(17): 3464. <https://doi.org/10.3390/app9173464>
 35. Singh A, Nakate U (2014) Microwave Synthesis, Characterization, and Photoluminescence Properties of Nanocrystalline Zirconia. *The Scientific World Journal* 2014.349457. <http://doi.org/10.1155/2014/349457>
 36. Zhang X, Zhang M, Zhang J, Zhang Q, Tsubaki N, Tan Y, Han Y (2019) Methane decomposition and carbon deposition over Ni/ZrO₂ catalysts: Comparison of amorphous, tetragonal, and monoclinic zirconia phase. *Int J Hydrogen Energy* 44(33):17887–17899. <https://doi.org/10.1016/j.ijhydene.2019.05.174>
 37. Aziz SB, Karim W, Brza M, Abdulwahid R, Raza SS, Al-Zangana S, Kadir M (2019) Ion Transport Study in CS: POZ Based Polymer Membrane Electrolytes Using Trukhan Model. *Int J Mol Sci* 20(21):5265. <https://doi.org/10.3390/ijms20215265>

38. Muhd JN, Ahmad Z, Md AH (2009) X-Ray Diffraction Studies of Cross Linked Chitosan With Different Cross Linking Agents For Waste Water Treatment Application. AIP Conf Proc 1202:106–111. <https://doi.org/10.1063/1.3295578>
39. Teimouri A, Nasab SG, Vahdatpoor N, Habibollahi S, Salavati H, Chermahini AN (2016) Chitosan /Zeolite Y/Nano ZrO₂ nanocomposite as an adsorbent for the removal of nitrate from the aqueous solution. Int J Biol Macromol 93:254–266. <https://doi.org/10.1016/j.ijbiomac.2016.05.089>
40. Kumar D, Pandey J, Kumar P (2018) Synthesis and characterization of modified chitosan via microwave route for novel antibacterial application. Int J Biol Macromol 107:1388–1394. <https://doi.org/10.1016/j.ijbiomac.2017.10.002>
41. Kołodziejka D, Krukowska J, Thomas P (2017) Comparison of sorption and desorption studies of heavy metal ions from biochar and commercial active carbon. Chem Eng J 307:353–363. <https://doi.org/10.1016/j.cej.2016.08.088>
42. Hassan HS, Elmaghraby EK (2019) Retention behavior of cesium radioisotope on poly (acrylamido-sulfonic acid) synthesized by chain polymerization. Appl Radiat Isot 146:40–47. <https://doi.org/10.1016/j.apradiso.2019.01.017>
43. Hassan HS, Abdel Maksoud MIA, Attia LA (2020) Assessment of zinc ferrite nanocrystals for removal of ¹³⁴Cs and ¹⁵²⁺¹⁵⁴Eu radionuclides from nitric acid solution. J Mater Sci: Mater Electron 31:1616–1633. <https://doi.org/10.1007/s10854-019-02678-y>
44. Puigdomenech I (2013) Make equilibrium diagrams using sophisticated algorithms (MEDUSA). Inorganic Chemistry. Royal Institute of Technology, Stockholm Sweden. <http://www.kemi.kth.se/medusa>. <https://sites.google.com/site/chemdiagr/>
45. Moloukhia H, Hegazy WS, Abdel-Galil E, Mahrous S (2016) Removal of Eu 3+, Ce 3+, Sr 2+, and Cs + ions from radioactive waste solutions by modified activated carbon prepared from coconut shells. Chem Ecol 32:324–345. <https://doi.org/10.1080/02757540.2016.1139089>
46. Ouyang D, Zhuo Y, Hu L, Zeng Q, Hu Y, He Z (2019) Research on the Adsorption Behavior of Heavy Metal Ions by Porous Material Prepared with Silicate Tailings. Minerals 9(5):291. <https://doi.org/10.3390/min9050291>
47. Dakrouy G, Abo-Zahra ShF, Hassan HS, Ali HEA (2020) Improvement of the sorption behavior of aluminum silicate composite toward ¹³⁴Cs and ⁶⁰Co radionuclides by non-living biomass of *Chlorella vulgaris*. Environ Sci Pollut Res 27:21109–21125. <https://doi.org/10.1007/s11356-020-08260-y>
48. Hassan HS, El-Kamash AM, Ibrahim HA (2019) Evaluation of hydroxyapatite/poly(acrylamide-acrylic acid) for sorptive removal of strontium ions from aqueous solution. Environ Sci Pollut Res 26:25641–25655. <https://doi.org/10.1007/s11356-019-05755-1>
49. Mu W, Chen B, Yu Q, Li X, Wei H, Yang Y, Peng S (2021) A novel zirconium phosphonate adsorbent for highly efficient radioactive cesium removal. J Mol Liq 326:115307. <https://doi.org/10.1016/j.molliq.2021.115307>
50. Ponou J, Wang LP, Dodbiba G, Okaya K, Fujita T, Mitsuhashi K, Atarashi T, Satoh G, Noda M (2014) Recovery of rare earth elements from aqueous solution obtained from Vietnamese clay minerals using dried and carbonized parachlorella. J Environ Chem Eng 2:1070–1081. <https://doi.org/10.1016/j.jece.2014.04.002>
51. Smičiklas I, Dimović S, Plečaš I (2007) Removal of Cs⁺, Sr²⁺ and Co²⁺ from aqueous solutions by adsorption on natural clinoptilolite. Applied Clay Science 35(1–2) :139–144. <https://doi.org/10.1016/j.clay.2006.08.004>
52. Saleh HM, Moussa HR, El-Saied FA, Dawoud M, Nouh EA, Abdel Wahed RS (2020) Adsorption of cesium and cobalt onto dried *Myriophyllum spicatum* L. from radio-contaminated water: Experimental and theoretical study. Progress in Nuclear Energy 125 (2020) 103393. <https://doi.org/10.1016/j.pnucene.2020.103393>
53. Hassan HS, Elmaghraby EK (2012) Preparation of graphite by thermal annealing of polyacrylamide precursor for adsorption of Cs(I) and Co(II) ions from aqueous solutions. Can J Chem 90(10):843–850. <https://doi.org/10.1139/v2012-058>
54. G William Kajjumba S Emik A Ongen H Kurtulus Ozcan S Aydın (2019) Modelling of adsorption kinetic processes—errors, theory and application. Adv Sorption Process Appl 1–19 <https://doi.org/10.5772/intechopen.80495>
55. Vijayaraghavan K, Jegan J, Palanivelu K, Velan M (2005) Biosorption of cobalt (II) and nickel (II) by seaweeds: batch and column studies. Separ Purif Technol 44:53–59. <https://doi.org/10.1016/j.seppur.2004.12.003>
56. Hai Wang T, Hsu Li M, Chun Yeh W, Yaw Wei Y, Ping Teng S (2008) Removal of cesium ions from aqueous solution by adsorption onto local Taiwan laterite. J Hazard Mater 160:638–642. <https://doi.org/10.1016/j.jhazmat.2008.03.050>
57. Braniša J, Jomova K, Lapčík L, Porubská M (2021) Testing of electron beam irradiated sheep wool for adsorption of Cr(III) and Co(II) of higher concentrations. Polym Testing 99:107191. <https://doi.org/10.1016/j.polymertesting.2021.107191>
58. Verma R, Asthana A, Singh AK, Prasad S (2017) An arginine functionalized magnetic nano-sorbent for simultaneous removal of three metal ions from water samples. RSC Adv 7:51079–51089. <https://doi.org/10.1039/C7RA09705K>

Publisher's Note Springer Nature remains neutral with regard to jurisdictional claims in published maps and institutional affiliations.